Journal of Solid State Chemistry **167,** 188–195 (2002)
doi:10.1006/jssc.2002.9641

Crystal Structure and Magnetic Properties of $SrCaMnGaO_{5+\delta}$

Peter D. Battle,*,[1] Anthony M. T. Bell,* Stephen J. Blundell,† Amalia I. Coldea,† Daniel J. Gallon,* Francis L. Pratt,‡ Matthew J. Rosseinsky,§ and Christopher A. Steer†

*Inorganic Chemistry Laboratory, Department of Chemistry, Oxford University, South Parks Road, Oxford OX1 3QR, United Kingdom; †Clarendon Laboratory, Department of Physics, Oxford University, Parks Road, Oxford OX1 3PU, United Kingdom; ‡ISIS, Rutherford Appleton Laboratory, Chilton, Didcot, Oxon. OX11 0QX, United Kingdom; and §Department of Chemistry, University of Liverpool, Liverpool L69 7ZD, United Kingdom

Received January 30, 2002; in revised form April 15, 2002; accepted May 3, 2002

The room-temperature crystal structure of the brownmillerite $SrCaMnGaO_{5+\delta}$ ($\delta = 0.035$) has been refined from neutron powder diffraction data; space group *Ima*2, $a = 15.7817(6)$, $b = 5.4925(2)$, $c = 5.3196(2)$ Å. Mn and Ga occupy 99.0(2)% of the 6- and 4-coordinate sites, respectively. A combination of magnetometry, neutron diffraction and μSR spectroscopy has shown that the compound orders magnetically at 180 K, and that the low-temperature phase has a G-type antiferromagnetic structure, with an ordered magnetic moment of 3.30(2) μ_B per Mn at 2 K. Displaced hysteresis loops provide evidence that the atomic moment has an additional, glassy component. Magnetometry shows that significant short-range magnetic interactions persist above 180 K, and μSR that the spin fluctuations are thermally activated in this temperature region. The compound is an electrical insulator which at 159 K shows an unusually large magnetoresistance of 85% in 6 T, increasing to 90% in 13 T.

Key Words: **brownmillerite; magnetoresistance.**

INTRODUCTION

There has been extensive recent interest in manganates, with the Ruddlesden–Popper (RP) phases of general formula $A_{n+1}B_nO_{3n+1}$ showing a fascinating range of structural, magnetic and electrical properties, notably colossal magnetoresistance (CMR) (1, 2). The observation of CMR in the $n = 2$ RP materials, often referred to as the naturally layered manganates, prompted attempts to synthesize other Mn-containing oxides having layered crystal structures, with the Mn analog of La_2CuSnO_6 being one of the target compounds. This cuprate adopts a structure (Fig. 1a) in which layers of vertex-sharing CuO_6 octahedra alternate with layers of SnO_6 octahedra along one of the axes of a pseudo-cubic perovskite unit cell (3). Thus, although the network of vertex-sharing octahedra is actually three dimensional, the unusual cation ordering pattern ensures that the electronically active Cu–O layers are isolated from each other, albeit imperfectly, by the intervening, electronically inactive Sn–O layers, thus giving a 2D aspect to the electronic properties of the material. Unfortunately, attempts to induce similar ordering between a d^{10} cation (Ga^{3+} or In^{3+}) and either Mn^{3+} or Mn^{4+} have been unsuccessful (4, 5). We have, therefore, turned our attention to materials having the brownmillerite (6) structure. These are essentially anion-deficient perovskites of stoichiometry $A_2B_2O_5$, with the anion vacancies ordering in chains along a $\langle 011 \rangle$ direction of the primitive cubic perovskite unit cell. This results in a structure having an orthorhombic unit cell $\sim 4a_p x \sim 2a_p \times 2a_p$ (a_p is the unit-cell parameter of the simple perovskite) with layers of BO_6 octahedra stacked alternately with layers of BO_4 tetrahedra along the x-axis. The introduction of a 1:1 mixture of two different metals on the B sites can lead to cation ordering, for example the structure (Fig. 1b) of $SrLaCuGaO_5$ is built up (7) from alternating layers of CuO_6 octahedra and GaO_4 tetrahedra. Thus, partial isolation of the electronically active, transition metal sheets is achieved. The detailed arrangement of the tetrahedral chains introduces some structural diversity into the brownmillerite family. As in $SrLaCuGaO_5$, the tetrahedra in successive layers can all take the same orientation (often described as –L–L–L– or –R–R–R–), which results in the space group *Ima*2, or order in alternating orientations (–L–R–L–R–) in space group *Pmcn*; the adoption of a disordered arrangement of two orientations results in space group *Imcm*. We describe below our attempts to use GaO_4 tetrahedra to isolate layers of MnO_6 octahedra in the system $Sr_{2-x}Ca_xMnGaO_{5+\delta}$, where the parameter δ is included to indicate that it is not always possible to prepare these phases in a fully reduced form. Others have been employing similar strategies, with Abakumov *et al.* (8) having found a mixture of the two ordered arrangements

[1] To whom correspondence should be addressed. Fax: +44-1865-272690. E-mail: peter.battle@chem.ox.ac.uk.

0022-4596/02 $35.00

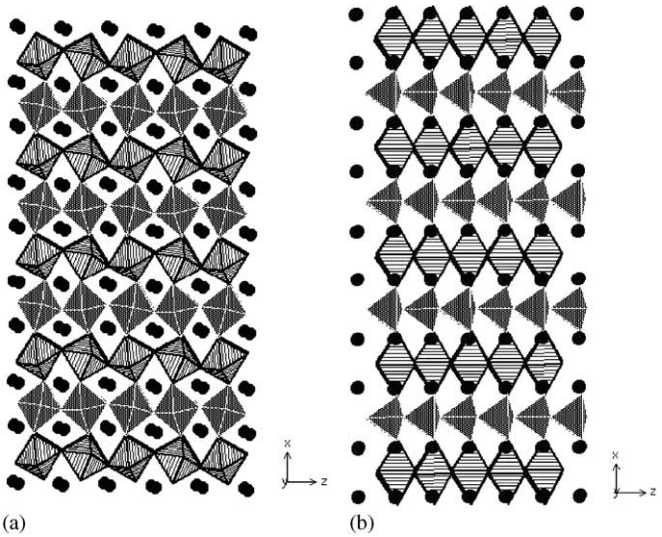

FIG. 1. Structures of (a) La_2CuSnO_6 and (b) $SrLaCuGaO_5$ showing Cu–O layers. CuO_6 occtahedra are hatched, SnO_6 octahedra or GaO_4 tetrahedra are shaded, filled circles represent Sr/La cations.

in $Ca_2MnGaO_{5+\delta}$ and Wright *et al.* (9) having reported a disordered arrangement in $Sr_2MnGaO_{5+\delta}$. However, a detailed study by Abakumov *et al.* (10) using electron microscopy has suggested that the tetrahedra in the latter phase are ordered in an –L–R–L–R– sequence within the layers, rather than in successive layers, thus creating a superlattice along one of the shorter axes of the brownmillerite unit cell. Preliminary measurements suggest that both compounds are antiferromagnetic at low temperatures. We have performed neutron diffraction experiments to provide a detailed description of the crystal and magnetic structures of $SrCaMnGaO_{5+\delta}$. We have also studied the magnetic properties of this phase by magnetometry and muon spin relaxation (μSR).

EXPERIMENTAL

We initially attempted to prepare Sr_2MnGaO_5 by standard ceramic synthesis methods, including the use of an inert atmosphere to stabilize the Mn^{3+} oxidation state. We were never able to obtain a pure brownmillerite sample of this composition, and we therefore began to substitute Sr^{2+} by Ca^{2+} in an attempt to produce a monophasic sample. We succeeded with the composition $SrCaMnGaO_{5+\delta}$, hence the focus on this phase in the remainder of this study. Stoichiometric quantities of $SrCO_3$, $CaCO_3$, Ga_2O_3, and MnO_2 were weighed out and ground together to prepare a 6 g sample of $SrCaGaMnO_5$. The reactants were fired overnight in air at 800°C before being pressed into 13 mm diameter pellets and heated for two periods of 48 h at 1200°C under flowing argon, ramping up to and down from the firing temperature at a rate of $10°C\,min^{-1}$. The sample was reground and checked by X-ray powder diffraction between firings. The quality of the final product was verified using X-ray data collected on a Siemens D5000 diffractometer, operating with $CuK\alpha_1$ radiation over the angular range $10° \le 2\theta \le 110°$ with a 2θ step size of 0.02°. The mean oxidation state of the Mn cations, and hence the oxygen content of the sample, was determined iodometrically. We estimate an error of 1.5% in x, where the Mn oxidation state is $2 + x$. Neutron powder diffraction data were recorded at 290 and 2 K using the diffractometer D2b at ILL, Grenoble, operating at a wavelength of 1.5938 Å over the angular range $0° \le 2\theta \le 150°$ with a 2θ step size of 0.05°. A sample of 5.1 g was contained in a vanadium can of diameter 8 mm, which was mounted in a standard ILL cryostat. The GSAS program suite (11) was used for Rietveld (12) analysis of all the diffraction data collected in this study; a pseudo-Voigt peak-shape function was used.

Magnetic measurements were performed using a Quantum Design SQUID magnetometer. The molar magnetic susceptibility was measured as a function of temperature over the range $5 \le T \le 350$ K; data were collected in fields of 100 and 1000 Oe after cooling the sample in zero applied field (ZFC) and after cooling in the measuring field (FC). The field dependence of the magnetization was studied over the range $-50 \le H \le 50$ kOe at a number of temperatures which were selected after inspection of the temperature dependence of the susceptibility. These data were collected after cooling the sample in a field of 50 kOe. Resistivity and magnetotransport measurements were carried out on a sintered bar using the four-wire method. The sample was mounted in a variable temperature insert which was located in a 16 T superconducting magnet. The applied current (<10 mA) was perpendicular to the applied magnetic field. μSR data were taken on the EMU pulsed muon beam-line at the ISIS facility at the Rutherford Appleton Laboratory. A beam of completely polarized muons was implanted with momentum 28 MeV/c into the sample under investigation. The muons stop suddenly ($<10^{-9}$ s) without loss of spin polarization. The muon decays, with a half-life of 2.2 μs, and emits a positron preferentially in the direction of the muon spin at the moment of decay. By measuring the number of counts (positrons) in a bank of forward and backward detectors, the emitted positron asymmetry is studied. The observed quantity is the time-dependent asymmetry, $A_\mu(t)$, which is proportional to the autocorrelation function of the muon spin polarization. The dynamics of the internal field are probed because the muon precesses around the instantaneous field direction. The Earth's magnetic field is compensated for to an accuracy of 10 μT.

RESULTS

Chemical analysis showed the mean oxidation state of the Mn in our sample to be 3.07(2), corresponding to the

composition $SrCaMnGaO_{5.035}$. Preliminary refinements of the crystal structure of $SrCaMnGaO_{5+\delta}$ against the neutron diffraction data collected at 290 K suggested that the tetrahedra adopt an ordered arrangement, with the same orientation in every layer (Fig. 1b), and that the structure is therefore best described in the non-centrosymmetric space group *Ima*2. Careful inspection of the peak profiles did not reveal any evidence for the presence of minority phases with a different ordering of the tetrahedra, as was found in $Ca_2MnGaO_{5+\delta}$. The contrasting neutron scattering lengths of Mn and Ga (−3.73 and 7.29 fm, respectively) resulted in a great sensitivity to the degree of cation ordering over the octahedral and tetrahedral sites, and we were able to show that 99.0(2)% of the former is occupied by Mn, with the same fraction of the latter being occupied by Ga. Similarly, the occupation factors of the anion sites all refined to be close to unity, the largest deviation being a value of 1.023(5) at the O2 site; these parameters were held fixed at unity in our final refinements.

TABLE 1
Refined Structural Parameters of $SrCaMnGaO_{5+\delta}$ in Space Group *Ima*2 at 290 and 2 K

		290 K	2 K
a (Å)		15.7817(6)	15.7705(2)
b (Å)		5.4925(2)	5.48090(7)
c (Å)		5.3196(2)	5.30562(6)
V (Å^3)		461.11(5)	458.600(7)
Sr/Ca	x	0.1114(1)	0.1112(1)
	y	0.0185(3)	0.0178(4)
	z	0.500(1)	0.500(1)
Mn	x	0	0
	y	0	0
	z	0	0
μ/μ_B			3.30(2)
Ga	x	$\frac{1}{4}$	$\frac{1}{4}$
	y	0.9305(4)	0.9318(4)
	z	−0.036(1)	−0.037(1)
O1	x	0.9924(1)	0.9929(1)
	y	0.2514(6)	0.2512(6)
	z	0.255(1)	0.255(2)
O2	x	0.1448(1)	0.1442(1)
	y	0.0538(3)	0.0537(4)
	z	0.027(1)	0.027(2)
O3	x	$\frac{1}{4}$	$\frac{1}{4}$
	y	0.6217(6)	0.6190(6)
	z	0.107(1)	0.107(1)
R_{wp} (%)		5.88	6.46
χ^2		5.3	6.4

TABLE 2
Atomic Displacement Parameters (Å^2) of $SrCaMnGaO_{5+\delta}$ at 290 and 2 K

		290 K	2 K
Sr/Ca	U_{11}	0.012(1)	0.012(1)
	U_{22}	0.005(1)	−0.0005(9)
	U_{33}	0.006(1)	0.002(1)
	U_{12}	−0.0004(7)	−0.0024(7)
	U_{13}	0.002(2)	0.003(2)
	U_{23}	0.000(1)	−0.002(1)
Mn	U_{iso}		0.0039(9)
	U_{11}	0.020(3)	
	U_{22}	0.001(2)	
	U_{33}	0.003(2)	
	U_{12}	−0.001(2)	
	U_{13}	0	
	U_{23}	0	
Ga	U_{iso}		0.0073(7)
	U_{11}	0.014(1)	
	U_{22}	0.004(1)	
	U_{33}	0.019(2)	
	U_{12}	0	
	U_{13}	0	
	U_{23}	0.005(1)	
O1	U_{11}	0.018(1)	0.017(1)
	U_{22}	0.0027(8)	−0.0006(8)
	U_{33}	0.0043(9)	0.0020(9)
	U_{12}	−0.001(1)	−0.001(1)
	U_{13}	−0.006(2)	−0.012(2)
	U_{23}	−0.0013(8)	0.0002(8)
O2	U_{11}	0.014(1)	0.013(1)
	U_{22}	0.009(1)	0.003(1)
	U_{33}	0.016(2)	0.010(2)
	U_{12}	0.0019(9)	0.0001(8)
	U_{13}	0.000(2)	−0.003(1)
	U_{23}	−0.001(1)	−0.001(1)
O3	U_{11}	0.023(2)	0.015(2)
	U_{22}	0.014(2)	0.009(2)
	U_{33}	0.008(2)	0.010(2)
	U_{12}	0	0
	U_{13}	0	0
	U_{23}	0.006(1)	0.006(1)

The refined structural parameters listed in Tables 1 and 2 are those that produced the satisfactory level of agreement between the observed and calculated diffraction patterns which is apparent in Fig. 2. Bond lengths derived from these parameters are listed in Table 3. The coordination geometry around the 4- and 6-coordinate sites is shown in Fig. 3.

Over the temperature range $205 \leq T \leq 350$ K the behavior of the molar magnetic susceptibility of $SrCaMnGaO_{5+\delta}$ is (Fig. 4) superficially that expected of a Curie–Weiss

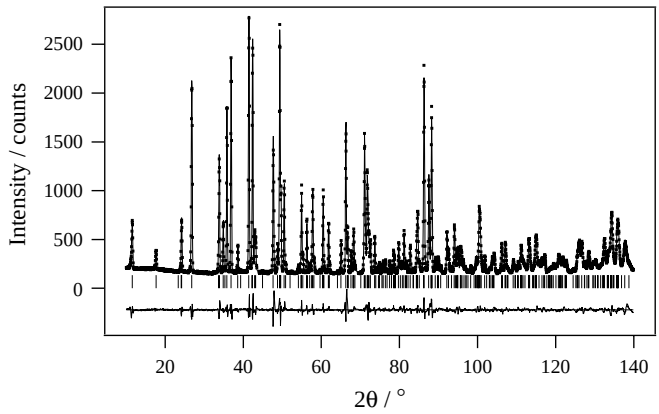

FIG. 2. Observed (·), calculated (–) and difference neutron powder diffraction profiles of $SrCaMnGaO_5$ at 290 K. Reflection positions are marked.

paramagnet, with a Curie constant $C = 4.61(7)\,cm^3\,K\,mol^{-1}$ (spin-only value for $Mn^{3+} = 3\,cm^3\,K\,mol^{-1}$) and a Weiss constant $\theta = -660$ K. There is clear evidence of a magnetic phase transition at 180 K, with the divergence of the ZFC and FC susceptibilities suggesting that the low-temperature phase is a weak ferromagnet. The magnetization (Fig. 5) is a linear, reversible function of applied field at 200 K, as is expected for a paramagnet, but hysteresis is detectable at 100 K, and is clearly apparent at 5 K. Moreover, the hysteresis loops are not symmetrical about the origin. The neutron diffraction pattern collected at 2 K (Fig. 6) showed additional Bragg scattering at low angles. This was assumed to be magnetic in origin and it was interpreted in terms of the magnetic structure drawn in Fig. 7. This is essentially the G-type antiferromagnetic structure adopted by many perovskites, although in this case the distance between the magnetic cations along x is approximately twice as large as it is in the yz plane. The

TABLE 3
Selected Bond Lengths (Å) in $SrCaMnGaO_{5+\delta}$

	298 K	2 K
Sr/Ca–O1 × 1	2.619(4)	2.611(4)
Sr/Ca–O1 × 1	2.564(4)	2.562(4)
Sr/Ca–O1 × 1	2.585(4)	2.580(4)
Sr/Ca–O1 × 1	2.640(4)	2.630(4)
Sr/Ca–O2 × 1	2.579(4)	2.573(3)
Sr/Ca–O2 × 1	2.858(4)	2.849(4)
Sr/Ca–O2 × 1	2.412(3)	2.410(3)
Sr/Ca–O3 × 1	2.388(3)	2.382(3)
Mn–O1 × 2	1.941(6)	1.932(6)
Mn–O1 × 2	1.890(6)	1.888(6)
Mn–O2 × 2	2.308(2)	2.299(2)
Ga–O2 × 2	1.824(2)	1.828(2)
Ga–O3 × 1	1.859(4)	1.878(4)
Ga–O3 × 1	1.919(4)	1.907(4)

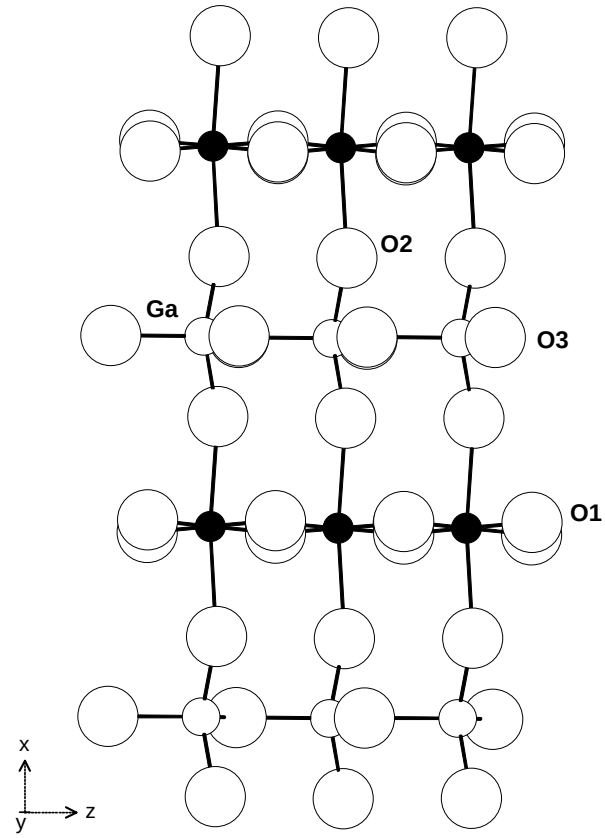

FIG. 3. Crystal structure of $SrCaMnGaO_5$ viewed along [010]. Filled circles represent Mn cations.

low-temperature crystal structure was refined in space group *Ima*2 and the resultant parameters and bond lengths are included in Tables 1–3. The ordered magnetic moment at the Mn sites was found to lie along x with a value of $3.30(2)\,\mu_B$. The refinement strategy was very similar to that used in the analysis of the room-temperature structure, although isotropic displacement parameters were applied to the Mn and Ga sites at 2 K.

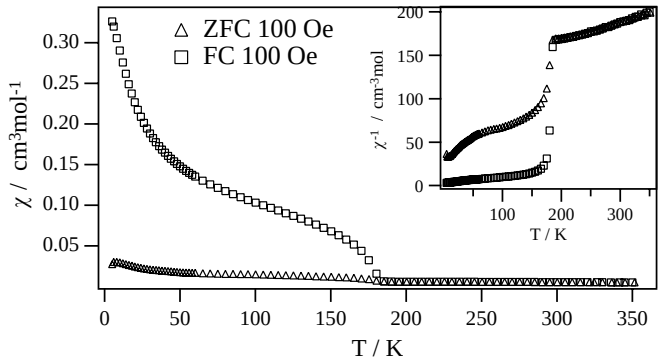

FIG. 4. Temperature dependence of the molar magnetic susceptibility of $SrCaMnGaO_5$, measured in a field of 100 G.

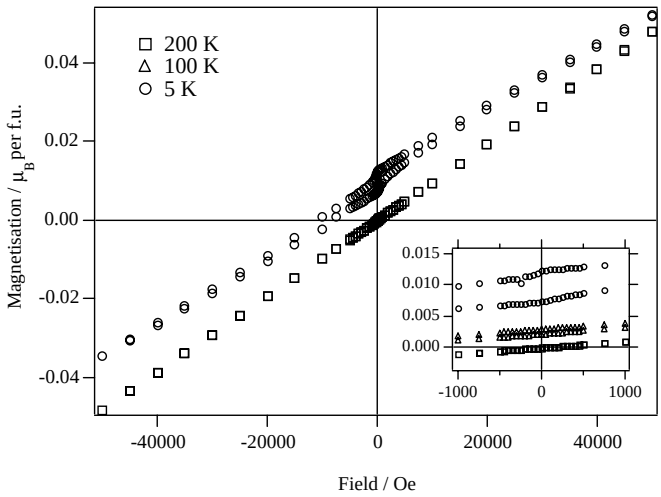

FIG. 5. Magnetization of $SrCaMnGaO_5$ as a function of applied field and temperature. For clarity, data taken at 100 K are only shown in the inset.

The results of fitting our μSR data to a stretched exponential form

$$A_\mu(t) = A_R \exp(-(\lambda\tau)^\beta) + A_{bg},$$

where the first term represents the contribution from the sample and the second term represents a small temperature-independent contribution from the sample holder, are shown in Fig. 8. Initial analyses in which both β and λ were free parameters always resulted in values of β close to 1 above the transition and close to 0.5 below the transition. In order to avoid correlations between the two parameters, only λ was varied in the final analyses, β being held equal to 1 above the transition (reflecting dynamics with a single correlation time) and equal to 0.5 below the transition (reflecting dynamics with a range of correlation times). This strategy resulted in good fits with normalized χ^2 values close to unity. There is a clear peak in the muon relaxation rate λ at 180 K (see Fig. 8b). This correlates with a sharp drop in the relaxing asymmetry A_R to approximately one-third of its high-temperature value which is observed at the same temperature (see Fig. 8a). This demonstrates that the local magnetic field sensed by the muon becomes static on the muon timescale below 180 K and corresponds to the divergence of the FC and ZFC susceptibilities. At temperatures above 180 K, we observe that the muon relaxation rate has an activated behavior with an energy of activation of 260(20) K (deduced from the non-zero intercept on the $T \ln \lambda$-axis in Fig. 8c). Below 180 K, we observe a slowly decreasing muon relaxation rate which maintains a relatively large value down to 40 K, indicative of the presence of slow dynamics persisting at these temperatures. The relaxation rate is very small and temperature-independent at very low temperatures.

The resistivity data (Fig. 9) show an activated behavior with an activation energy of 630.4(3) K in zero field. The compound is an electrical insulator which at 159 K shows a magnetoresistance of 85% in 6 T, increasing to 90% in 13 T; the zero field conductivity of the sample was too low to be measured at lower temperatures with the apparatus

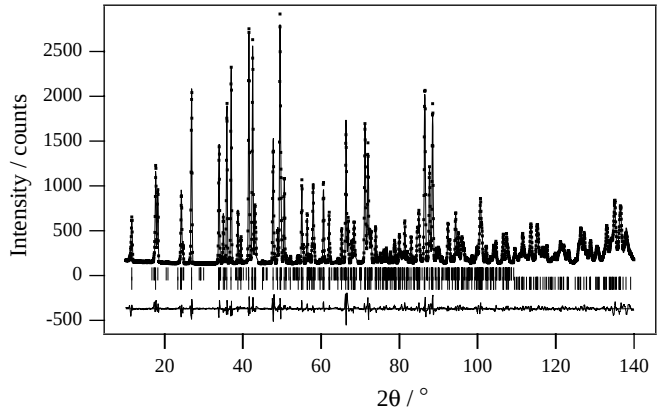

FIG. 6. Observed (·), calculated (–) and difference neutron powder diffraction profiles of $SrCaMnGaO_5$ at 2 K. Positions of both magnetic (upper) and structural (lower) reflections are marked.

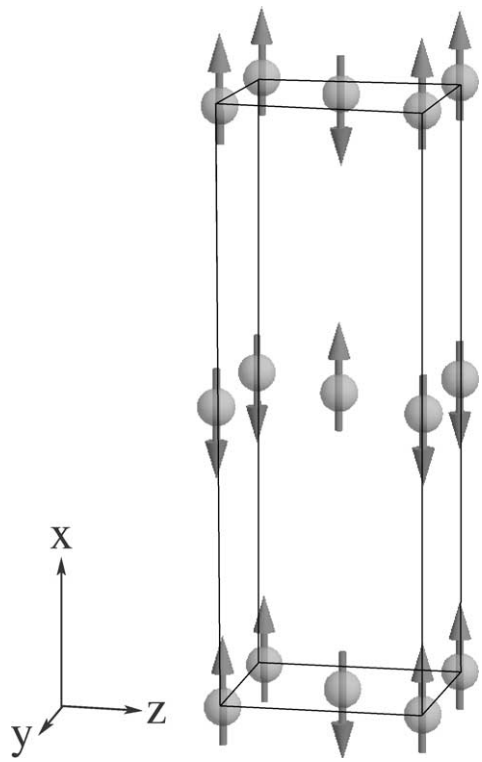

FIG. 7. Magnetic unit cell of $SrCaMnGaO_5$; only Mn cations are shown.

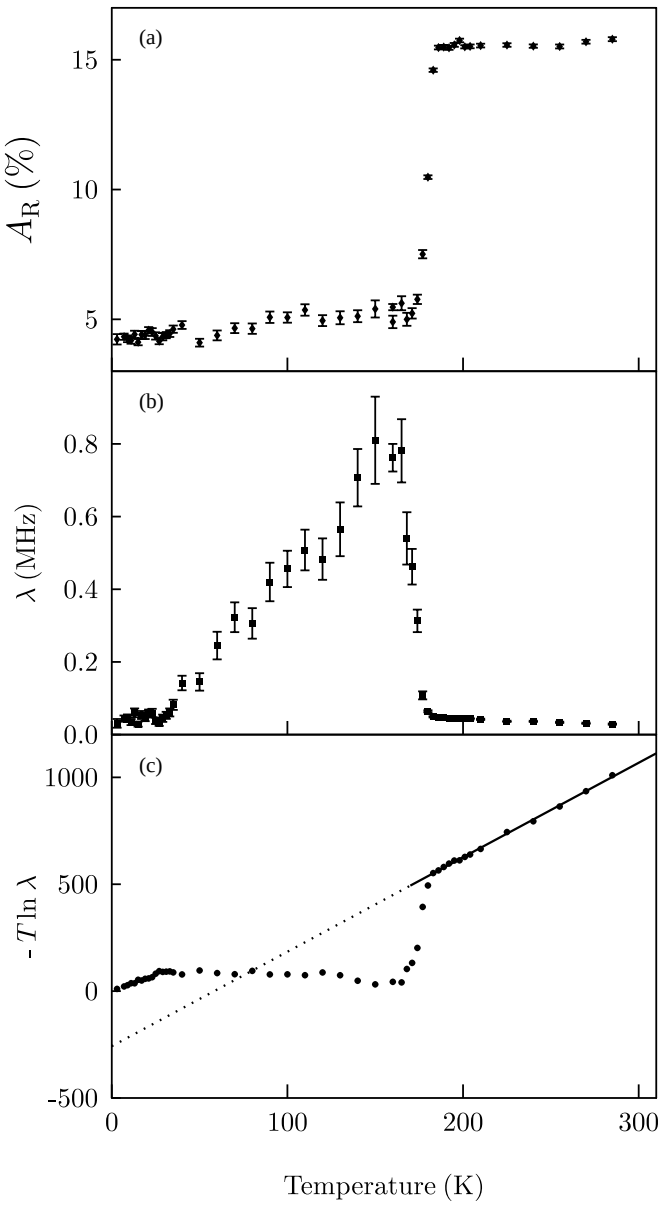

FIG. 8. Temperature dependence of the μSR parameters: (a) the relaxing asymmetry A_r, (b) the relaxation rate λ, (c) λ, plotted to emphasize the activated behaviour above 180 K.

available. The magnetoresistance decreases with increasing temperature but persists above the magnetic ordering temperature. An inflection is apparent at that temperature in 6 T but not in 13 T, and in both cases, the temperature dependence of the magnetoresistance is less marked above 210 K. In a field of 13 T, the sample shows an activated behavior below the transition temperature with an activation energy of 446.73(7) K, and above the transition, the data can be fitted to a two-dimensional variable range hopping law ($\rho = \rho_0 \exp((T_0/T)^{1/3})$ with parameters $\rho_0 = (2.178 \pm 0.005) \times 10^{-12}\,\Omega\,\mathrm{cm}^{-1}$ and $T_0 = 9.591(8) \times 10^5\,\mathrm{K}$.

DISCUSSION

The degree of oxidation in our sample of SrCa $MnGaO_{5.035}$ is clearly intermediate between that found in $Ca_2MnGaO_{5.045}$ and that in $Sr_2MnGaO_{4.97}$, the latter two

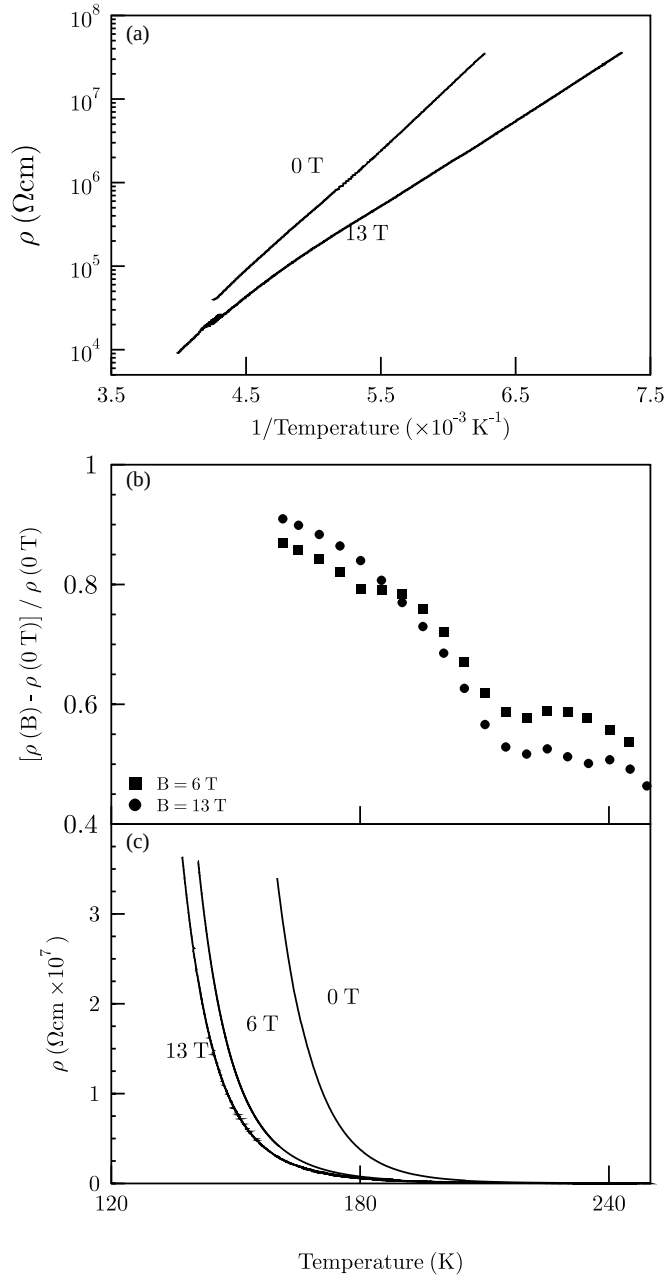

FIG. 9. (a) Resistivity of $SrCaMnGaO_5$ as a function of inverse temperature at 0 and 13 T, (b) magnetoresistance in 6 and 13 T as a function of temperature, (c) resistivity as a function of temperature and applied field.

samples having been prepared by Abakumov *et al.* (8, 10) in sealed, evacuated tubes. However, the error in the Mn oxidation state is too high to permit us to consider the difference between the two Ca-containing samples to be significant. It is interesting to note that Abakumov *et al.* chose to prepare $Sr_2MnGaO_{5+\delta}$ in a sealed tube, and that we were unable to prepare a pure sample of $Sr_2MnGaO_{5+\delta}$ under Ar, although Wright *et al.* (9) have reported the preparation of a sample of Sr_2MnGaO_5 with $\delta \sim 0$ under N_2. Abakumov *et al.* were unable to prepare pure $Ca_2MnGaO_{5+\delta}$ without the use of sealed tubes, and even then their product contained two brownmillerite phases in ratio of 82:18; we found no evidence to suggest that our mixed Ca/Sr sample, prepared under flowing Ar, was biphasic. These variations emphasize the importance of subtle changes in the experimental conditions during the synthesis of brownmillerite phases.

The tetrahedra in $SrCaMnGaO_{5.035}$ order in the same manner as those in the minority phase in $Ca_2MnGaO_{5+\delta}$. The same pattern was revealed in an X-ray powder diffraction study of $Sr_2MnGaO_{4.97}$, although that experiment suggested that further complexities might be present and electron diffraction revealed superlattice formation perpendicular to [1 0 0]. The analogous sample prepared by Wright *et al.* was described as having a disordered array of tetrahedra–further evidence of the dependence of the structural chemistry of these systems on the method of synthesis. The –L–L–L– (*Ima*2) tetrahedral ordering sequence has also been observed in, for example, $LaSrCuGaO_5$ (7) and $Sr_2Fe_2O_5$ (13), although the latter has also been described in *Imcm* (14), thus demonstrating that the Mn/Ga system is not the only one to adopt more than one tetrahedral ordering scheme. The X-ray evidence for disorder or superlattice formation in $Sr_2MnGaO_{4.97}$ was contained in the high displacement parameters of the O^{2-} ions in the tetrahedral layer, and the unusually short bonds between these anions and Ga^{3+}; these anomalies are not present in $SrCaMnGaO_{5.035}$ and it, therefore, seems unlikely that superlattice formation occurs in this material. The anisotropic nature of the brownmillerite structure facilitates the accommodation of cations with degenerate electronic ground states that might be expected to cause a Jahn–Teller distortion. Even in the Fe^{3+} compound $Sr_2Fe_2O_5$, the metal–oxygen bond lengths at the 6-coordinate site range from 1.879 to 2.162 Å (13), but when a Jahn–Teller cation is present, as in $SrCaMnGaO_{5.035}$, the range extends from 1.890 to 2.308 Å, with the strain parameter

$$\sigma_{JT} = \sqrt{\frac{1}{6}\sum_i [(B\text{–O})_i - \langle B\text{–O}\rangle]^2}$$

increasing from 0.103 to 0.186. The magnitude of this distortion justifies the decision to use the structure to produce a pseudo-2D Mn–O system, and it is interesting to note (Fig. 3) that the Mn–O layers are relatively flat, with O1–Mn–O1 and Mn–O1–Mn bond angles of 179.1(4)° and 172.7(1)°, respectively. The mean Ga–O bond length (1.857 Å) is longer than that (1.83 Å) determined from $LaSrCuGaO_5$, although that determination was made with a relatively low precision. The Ga–O3 bonds within the Ga–O sheets are significantly longer than those (Ga–O2) which link the tetrahedra to the octahedra, the compression of the latter facilitating the extension of the octahedra perpendicular to the layers. We note that the model used to describe the structure of $SrCaGaMnO_5$ is much simpler than that needed to describe Ca_2GaMnO_5 (8), although the fit to our data is slightly better and the bond lengths are at least as precise. We believe that the 1:1 Sr:Ca phase is structurally simpler than the phases containing only Sr or Ca.

Although the magnetic behavior of $SrCaMnGaO_{5.035}$ above 200 K can be described by the Curie–Weiss law, the enhanced value of the Curie constant suggests that it is inappropriate to treat the sample as an ideal paramagnet in this temperature region, where short-range ordering is likely to persist. The μSR data also show that, for $180 \leq T \leq 300$ K, the spin fluctuations are governed by an activated process which we associate with crystal-field effects experienced by the non-spherical Mn^{3+} cations. Similar effects, associated with rare-earth crystal fields, were observed (15) in μSR experiments on $Sr_2LnMn_2O_7$ where *Ln* is a lanthanide cation other than spherical Gd^{3+}. The onset of long-range magnetic ordering at 180 K is clear in both the susceptibility and the muon data, with the former suggesting the formation of a canted antiferromagnetic phase. However, the displaced hysteresis loops in Fig. 5 show that there is also a glassy component to the magnetism, a conclusion which is consistent with the relatively slow decrease in the muon relaxation rate seen in Fig. 8b. This could arise from the Ga/Mn cation disorder (~1%) or from the presence of some Mn^{4+} cations (7%) as described above. We do not have a clear explanation for the upturn in the temperature dependence of the susceptibility which is seen below 50 K, but the observation of a low-temperature transition in the muon data, clearly seen in Fig. 8c, demonstrates that it is from the bulk sample rather than a minor impurity phase. The antiferromagnetic structure deduced from the neutron diffraction data collected at 2 K is the same as that found in other brownmillerites, for example $Ca_2Fe_2O_5$ (16); in both cases, the ferromagnetic component of the structure is too weak to be measured in a neutron powder diffraction experiment. However, the ordering temperature (180 K) is markedly reduced from the value of 720 K found in the Fe-containing compound. The reduction can be attributed in part to the lower concentration of magnetic cations which effectively reduces the dimensionality of the magnetic structure from 3 to 2, although the reduced

occupancy of the cation *d* orbitals will also be a factor. The reduction of the ordered magnetic moment of the Mn^{3+} cations ($3.30\,\mu_B$) below the spin-only value can be largely attributed to the effects of covalency. Interestingly, the pseudo-2D phase $SrLaMnO_4$ also has (17) a Néel temperature of 180 K, but the ordered magnetic moment in that case is reduced to the surprisingly low value of $0.8\,\mu_B$, suggesting that the frustration present in the K_2NiF_4 structure, but not in brownmillerite, has a significant effect. $Sr_2Mn_2O_5$, not a brownmillerite but containing MnO_5 pyramids created by a different oxide-vacancy ordering scheme (18), has an unfrustrated 3D structure with $T_N = 375\,K$ and $\mu_{Mn} = 3.44\,\mu_B$.

The non-metallic nature of $SrCaGaMnO_{5.035}$ is consistent with the presence of a low oxygen excess and the presence of one dominant oxidation state for the transition metal cation; the splitting of the e_g band caused by the Jahn–Teller distortion at the Mn site ensures that the compound is an insulator. The use of a polycrystalline sample leaves us unable to distinguish between intergrain and intragrain effects when considering the magnetoresistance, but the observation of high magnetoresistance in a layered insulator is reminiscent of the behavior of the $n = 2$ Ruddlesden–Popper (RP) phase $Sr_2NdMn_2O_7$ (19). The magnetism of the RP phases was originally thought to show 2D effects at $\sim 270\,K$, but the observed magnetization increase has subsequently been ascribed to the presence of perovskite intergrowths (20, 21). There is no comparable evidence for the presence of such intergrowths in $SrCaGaMnO_{5.035}$ and it is, therefore, interesting that the conductivity above the ordering temperature in a field of 13 T is well described by a 2D model. Attempts to increase the conductivity by reducing the concentration of oxygen vacancies produced changes in the structure and magnetic properties of $SrCaGaMnO_5$ which were very similar to those observed by Abakumov *et al.* (10) in the case of $Sr_2MnGaO_{5+\delta}$; these results will be described in more detail elsewhere.

ACKNOWLEDGMENTS

We are grateful to EPSRC for financial support, and to Thomas Hansen for experimental assistance at ILL.

REFERENCES

1. A. P. Ramirez, *J. Phys.: Condens. Matter* **9,** 8171 (1997).
2. P. D. Battle and M. J. Rosseinsky, *Curr. Opin. Solid State Mater. Sci.* **4,** 163 (1999).
3. M. T. Anderson and K. R. Poeppelmeier, *Chem. Mater.* **3,** 476 (1991).
4. P. D. Battle, A. I. Coldea, N. A. Jordan, M. J. Rosseinsky, and J. Singleton, *J. Mater. Chem.* **11,** 1656 (2001).
5. E. J. Cussen, M. J. Rosseinsky, P. D. Battle, J. C. Burley, L. E. Spring, J. F. Vente, S. J. Blundell, A. I. Coldea, and J. Singleton, *J. Am. Chem. Soc.* **123,** 1111 (2001).
6. W. C. Hansen, L. T. Brownmiller, and R. H. Bogue, *J. Am. Chem. Soc.* **50,** 396 (1928).
7. J. T. Vaughey, J. B. Wiley, and K. R. Poeppelmeier, *Z. Anorg. Allg. Chem.* **598,** 327 (1991).
8. A. M. Abakumov, M. G. Rozova, B. P. Pavlyuk, M. V. Lobanov, E. V. Antipov, O. I. Lebedev, G. vanTendeloo, D. V. Sheptyakov, A. M. Balagurov, and F. Bourée, *J. Solid State Chem.* **158,** 100 (2001).
9. A. J. Wright, H. M. Palmer, P. A. Anderson, and C. Greaves, *J. Mater. Chem.* **11,** 1324 (2001).
10. A. M. Abakumov, M. G. Rozova, B. P. Pavlyuk, M. V. Lobanov, E. V. Antipov, O. I. Lebedev, G. vanTendeloo, O. L. Ignatchik, E. A. Ovtchenkov, Y. A. Koksharov, and A. N. Vasil'ev, *J. Solid State Chem.* **160,** 353 (2001).
11. A. C. Larson and R. B. von-Dreele, "General Structure Analysis System (GSAS)," Los Alamos National Laboratories, Report LAUR 86-748, 1990.
12. H. M. Rietveld, *J. Appl. Crystallogr.* **2,** 65 (1969).
13. M. Harder and H. Müller-Buschbaum, *Z. Anorg. Allg. Chem.* **464,** 169 (1980).
14. C. Greaves, A. J. Jacobson, B. C. Tofield, and B. E. F. Fender, *Acta Crystallogr. B* **31,** 641 (1975).
15. R. I. Bewley, S. J. Blundell, B. W. Lovett, T. Jestädt, F. L. Pratt, K. H. Chow, W. Hayes, P. D. Battle, M. A. Green, J. E. Millburn, M. J. Rosseinsky, L. E. Spring, and J. F. Vente, *Phys. Rev. B* **60,** 12,286 (1999).
16. T. Takeda, Y. Yamaguchi, S. Tomiyoshi, M. Fukase, M. Sugimoto, and H. Watanabe, *J. Phys. Soc. Jpn.* **24,** 446 (1968).
17. S. Kawano, N. Achiwa, N. Kamegashira, and M. Aoki, *J. Phys.* **49,** Colloques C8 829 (1988).
18. T. Mori, K. Inoue, N. Kamegashira, Y. Yamaguchi, and K. Ohoyama, *J. Alloys Comp.* **296,** 92 (2000).
19. P. D. Battle, S. J. Blundell, M. A. Green, W. Hayes, M. Honold, A. K. Klehe, N. S. Laskey, J. E. Millburn, L. Murphy, M. J. Rosseinsky, N. A. Samarin, J. Singleton, N. A. Sluchanko, S. P. Sullivan, and J. F. Vente, *J. Phys.: Condens. Matter* **8,** L427 (1996).
20. S. D. Bader, R. M. Osgood, D. J. Miller, J. F. Mitchell, and J. S. Jiang, *J. Appl. Phys.* **83,** 6385 (1998).
21. J. Sloan, P. D. Battle, M. A. Green, M. J. Rosseinsky, and J. F. Vente, *J. Solid State Chem.* **138,** 135 (1998).